Dose calculation models for proton treatment planning using a dynamic beam delivery system: an attempt to include density heterogeneity effects in the analytical dose calculation

Phys. Med. Biol. **44** (1999) 27–41. Printed in the UK PII: S0031-9155(99)95541-0

Dose calculation models for proton treatment planning using a dynamic beam delivery system: an attempt to include density heterogeneity effects in the analytical dose calculation

Barbara Schaffner, Eros Pedroni and Antony Lomax
Division of Radiation Medicine, Paul Scherrer Institute, 5232 Villigen-PSI, Switzerland

Received 30 June 1998, in final form 2 October 1998

Abstract. The gantry for proton radiotherapy at the Paul Scherrer Institute (PSI) is designed specifically for the spot-scanning technique. Use of this technique to its full potential requires dose calculation algorithms which are capable of precisely simulating each scanned beam individually. Different specialized analytical dose calculations have been developed, which attempt to model the effects of density heterogeneities in the patient's body on the dose. Their accuracy has been evaluated by a comparison with Monte Carlo calculated dose distributions in the case of a simple geometrical density interface parallel to the beam and typical anatomical situations. A specialized ray casting model which takes range dilution effects (broadening of the spectrum of proton ranges) into account has been found to produce results of good accuracy. This algorithm can easily be implemented in the iterative optimization procedure used for the calculation of the optimal contribution of each individual scanned pencil beam. In most cases an elemental pencil beam dose calculation has been found to be most accurate. Due to the long computing time, this model is currently used only after the optimization procedure as an alternative method of calculating the dose.

1. Introduction

World-wide interest in proton radiotherapy is increasing. This is due to the fact that protons have a well defined range in homogeneous tissue and deposit most of their energy at the end of their range in the so-called Bragg peak. Thus, a single incident proton beam can be modulated to produce a flat high-dose region—the spread-out Bragg peak—at any depth of the body with a lower dose in the entrance region. No dose is deposited past the distal border of the spread-out Bragg peak. With this characteristic depth-dose curve, protons have a considerable potential for sparing normal tissue surrounding a tumour.

The uncertainty created by multiple Coulomb scattering on the trajectories of protons traversing complex density distributions is the most important effect limiting the precision of analytical dose calculation algorithms in proton radiotherapy. The best solution is to model these effects with Monte Carlo simulations, which are becoming more and more available for the specific needs of radiotherapy treatment planning. Many papers published by various authors (Petti 1992, 1996, Ragona *et al* 1997, Tourovsky *et al* 1993) demonstrate the interest in this field. However, there are still strong reasons to continue to use analytical calculations and also to improve them in the future:

(i) Simple analytical calculations are still considerably faster than MC simulations. This is important during the planning process to get a quick overview of the dose distributions obtained at different gantry angles.

0031-9155/99/010027+15$19.50

(ii) In body regions without critical heterogeneities a good analytical dose calculation is usually accurate enough.

(iii) The treatment planning system used at PSI for the spot-scanning system is based on an iterative optimization of the contributions of individual spots for one beam direction at a time (Scheib 1993, Scheib *et al* 1994, Lomax *et al* 1996). A recently developed code (Lomax 1999) allows the optimization of individual pencil beams from multiple beam directions. For these applications only an analytical spot by spot dose calculation algorithm can be used. The quality of the treatment will depend strongly on the precision of the dose algorithm.

The first dose calculation algorithms for the treatment planning of proton radiotherapy were written for scattered beam techniques and use a broad-beam ray casting technique (Chen *et al* 1979). Compensation for tissue heterogeneities is implemented by compensating boluses as described by Koehler *et al* (1975) and Urie *et al* (1984). The capabilities of modelling and possibly correcting for the effects of range dilution were very limited.

At PSI a spot-scanning system for a compact proton gantry has been developed (Pedroni *et al* 1995). The compensation for tissue heterogeneities is achieved through the energy modulation of the individual pencil beams by moving polyethylene plates dynamically into the beam (range shifter). We hope that the flexibility to vary the dose locally at each spot can be used to compensate at least partially for the effects of range dilution. For the spot-scanning, a dedicated treatment planning system has been developed (Scheib and Pedroni 1992, Scheib 1993, Scheib *et al* 1994), which uses a physical model of the scanned beam based on measurements of the physical pencil beam in water and in air. The dose distribution of the scanned beam is scaled in depth according to the density integrated along the central axis of the beam spot. Since the physical pencil beam at PSI is relatively large (6–8 mm FWHM), it has been found that neglecting density variations across the pencil beam can lead to considerable errors in the dose distribution.

A solution for better modelling the dose distribution obtained by both scattered and scanned beams is the use of elemental pencil beam models. They are conceptually the same as the scanned pencil beam model but with an infinitesimally small phase space. Broad scattered beams (Petti 1992, 1996, Hong *et al* 1996) and scanned beams are then modelled as a superposition of elemental pencil beams. Another solution is to apply the ray casting technique to the physical scanned beam.

An elemental pencil beam, as well as two modified ray casting versions of the original PSI scanning beam, have been developed for the PSI spot-scanning technique. Their results have been evaluated by comparing them with the results of the PSI Monte Carlo code (Tourovsky *et al* 1993) for both an idealized density interface (a slab of bone in water) and anatomical situations.

2. The basic theory for the modelling of scanned pencil beams

2.1. The characteristics of the physical scanned beam

The characteristics of the physical scanned beam are modelled from measurements in water and in air (Scheib and Pedroni 1992, Scheib 1993, Scheib *et al* 1994). Details about the physical dose model, the measurements of its basic data, its present use for treatment planning at PSI, including its validation through routine dosimetric verification of each dose field in geometrical phantoms, go beyond the scope of this work, which was to improve the way of treating density heterogeneity effects in our treatment planning. Only a short summary shall be given here for a better understanding.

Our dose calculation consists of a superposition of individual scanned pencil beams. The description of the physical pencil beam uses calculated look-up tables of the depth-dose curve and the depth–width relation of a proton beam in water. The depth-dose curve is characterized by the nominal beam energy and the width of the initial energy spectrum (momentum band). The dose deposited by a single proton of known initial energy is derived from the Bethe–Bloch equation (Bichsel 1972). A discrete sampling of the energy spectrum is used to obtain the depth dose deposited by an average proton. An extra component is added to the initial energy spectrum to account for range straggling in the patient. Nuclear interactions are modelled as a fluence reduction of primary protons and an empirical model for the residual dose deposited by charged secondaries is used. The beam width due to multiple Coulomb scattering is modelled based on the work by Øverås (1960), in which the magnitude of the scattering is integrated as a function of depth. Contributions from the width of the incident beam and the combined effect of range shifter plates and the air gap to the patient are added quadratically. The look-up tables describing the integral dose and width of the beam as a function of the depth in the patient are finally obtained by fitting very few parameters to the model to coincide precisely with the corresponding direct measurements of the actual pencil beam. The same look-up-tables are also used as input data to the PSI Monte Carlo code, which will be used here as a reference. The exact agreement between analytical calculation, Monte Carlo and the measurements in the case of a homogeneous medium (water) has been carefully checked before starting the investigation on density heterogeneity effects discussed in this paper.

In this description the formula for the dose deposited at a position (x, y, z) by a pencil beam along the z-axis and positioned at (x_0, y_0) is given by

$$D(x, y, z) = N_{\mathrm{p}^+}\mathrm{ID}(\mathrm{wer})\frac{1}{2\pi\sigma_x\sigma_y}\exp[-(x_0 - x)^2/2\sigma_x^2]\exp[-(y_0 - y)^2/2\sigma_y^2] \tag{1}$$

where

$$\mathrm{wer} = \mathrm{wer}(x_0, y_0, z)$$
$$\sigma_i = \sigma_i(\mathrm{wer}(x_0, y_0, z)) \quad \text{with} \quad i = x, y.$$

ID is the integral dose, interpolated from the depth-dose look-up table, N_{p^+} is the number of protons in the beam spot, wer is the total water-equivalent range (range shifter plates plus patient) along the central axis of the beam and σ_x, σ_y are the standard deviations of the Gaussians in x and y directions. They include all contributions to the beam width, i.e. initial phase space, Coulomb scattering in the patient and range shifter and its propagation in the air gap between range shifter and patient.

This description of the physical pencil beam was originally used as the dose calculation model for treatment planning (Scheib 1993) with the assumption that the phase space, i.e. especially the width of the scanning pencil beam, is small compared with the broadening of the beam due to multiple Coulomb scattering. Since the water-equivalent range was only calculated along the axis of the scanning pencil beam, off-axis heterogeneities are not taken into account in the calculation of the dose deposited by the scanned pencil beam. With zero phase space this model would be the same as an elemental pencil beam model. In practice, however, the beam width due to the phase space can be quite large, especially when a large number of range shifter plates and a large air gap between gantry nozzle and patient are used.

The problems introduced by the large phase space in the presence of density heterogeneities can be clearly demonstrated when comparing the physical beam model with the results of the Monte Carlo simulation for a geometrical test situation consisting of a 2 cm thick slab of 'cortical bone' (stopping power 1.8 relative to water) in water. A single beam passes along the interface between the slab and water. For this calculation an initial beam energy of 177 MeV, an

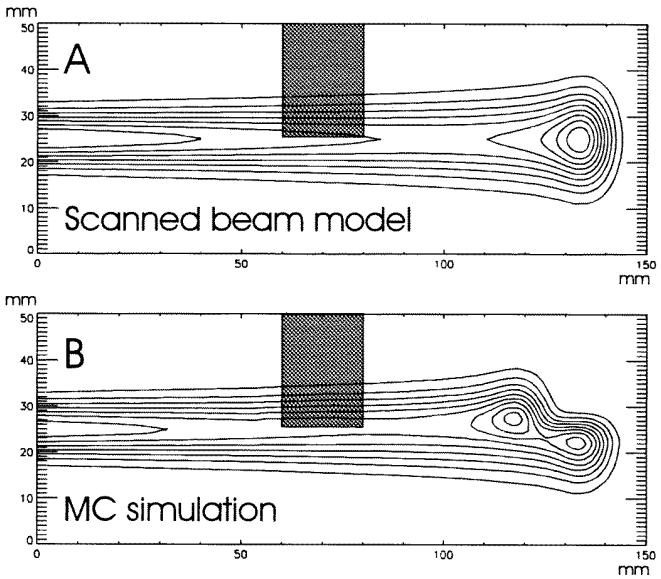

Figure 1. Result of the original scanned beam model (A) compared with a Monte Carlo calculated dose distribution (B) for the test situation (177 MeV, 15 range shifter plates, air gap of 10 cm). The scanned beam model is inadequate for this situation since the influence of the high-density slab is not modelled.

air gap of 10 cm and 15 range shifter plates ($\simeq$ 6.8 cm of water) were chosen. The resolution of the dose calculation grid is 1 mm. Since this original model only used the density information along the central axis of the beam, the dose calculation completely disregards the density heterogeneity of the slab and therefore corresponds to the dose of a whole pencil beam in water. This is shown as an isodose line display in figure 1A.

A comparison with the result of the PSI Monte Carlo code (figure 1B) shows that there are large dose errors in the shadow of the slab. Due to the limitations of this approach this model will not be considered further. Instead, new algorithms, based on the physical characteristics of the scanned beam described above, were developed to better account for heterogeneities.

2.2. Estimation of the range dilution after density heterogeneities

When protons pass through inhomogeneous tissue, their initially well defined Bragg peak becomes degraded (Urie *et al* 1986, Schneider and Pedroni 1995). Due to the high dose deposited in the peak region, this degradation, which is caused by a dilution of the proton ranges, has a strong influence on the final dose distribution. It is therefore important to model this effect in the treatment planning with the highest possible precision. For this purpose we have developed a simple algorithm which can be used to estimate range dilution of the Bragg peak in the presence of density heterogeneities.

For a given beam incidence, we define the range dilution of a proton beam passing through a heterogeneous medium to be the root mean square (rms) of the range of protons stopping at a given point P. The water-equivalent proton ranges are calculated from the CT data set by using representative straight proton trajectories centred at point P. The angular spacing and weighting of those individual rays is chosen to represent a Gaussian distribution, whose sigma is determined by the rms of the angular distribution of the proton trajectories (angular spread) resulting from both the effective phase space and multiple Coulomb scattering in the patient.

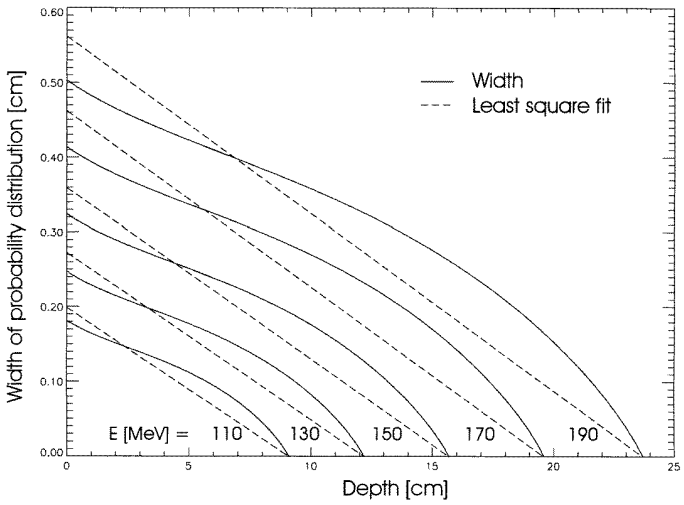

Figure 2. Root mean square (rms) width of the probability distribution of the lateral displacement as a function of depth of all possible trajectories of protons stopping at the same point, plotted for different initial energies. Least square fits were done through the stopping point to approximate the width–depth relationship with a straight line. The gradient of the fits was found to be almost a constant for the energies relevant for radiotherapy.

In this model for the range dilution we make the following assumptions:

(i) The beam (a scanned or scattered proton field) is assumed to extend infinitely in the lateral directions.

(ii) Only protons stopping at point P are considered, since they cause the largest errors in the dose calculation.

(iii) The representative trajectories are straight lines.

A similar approach has been taken by Schneider *et al* (1998). They showed a good coincidence between the range spectra obtained from their analytical calculation and the Monte Carlo simulation.

The *angular spread* can be separated in two components (Schaffner 1997):

(i) *Angular spread of the effective phase space*. We define the effective phase space to be the properties of the incident proton beam in air after any beam-modifying devices (modulator wheel or range shifter plates). The angular spread of the effective phase space of an infinitely extended beam is constant at any depth in the patient but depends on the parameters of the beam delivery system.

(ii) *Multiple Coulomb scattering in the patient*. Multiple Coulomb scattering in the patient causes the path of the protons to deviate from a straight line. Although the 'local' scattering angle varies as a function of depth, for simplicity we defined a single 'effective' scattering angle to approximate the cumulated effect of multiple Coulomb scattering over the whole proton range through the patient. To determine this angle the probability distribution of all possible trajectories stopping at a certain point P in the patient were calculated. The rms width of this distribution is plotted as a function of depth for different energies in figure 2. A least-square fit was applied to approximate the width versus depth relations by straight lines for different energies. The angular spread due to multiple Coulomb scattering was defined to be the slope of that line. It was found that this approach yields an almost constant angle of 1.3° for initial energies from 110–190 MeV. This component of the angular spread is an intrinsic property of protons and does not depend on the application technique.

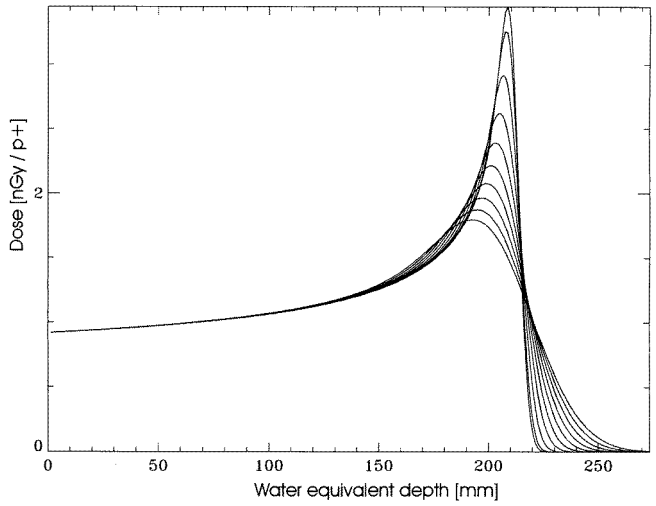

Figure 3. Depth dose curve for a 177 MeV beam with a momentum band of 1.1% and with a relative range dilution of 0–9% in steps of 1%.

The *total angular spread* (σ_ϕ) is defined as the squared sum of the contribution from effective phase space and multiple Coulomb scattering in the patient. It is a function of the initial phase space and the amount of material in the beam path. In the case of the PSI system, the amount of material in the beam path is defined by the number of range shifter plates.

The range dilution effect on the dose can be simulated as a broadening of the initial energy spectrum. The resulting depth dose curves for a relative range dilution from 0% to 9% standard deviation are shown in figure 3. The influence of range dilution on the shape of the Bragg curve is very high in the peak region, while there are almost no changes in the plateau. This underlines the importance of the peak region and justifies our approach of calculating the range dilution only for protons stopping in the point of interest.

3. Analytical dose calculation models

3.1. A ray casting model specialized for spot-scanning

Our first approach to model off-axis heterogeneities is to apply a ray casting technique to the original physical scanned beam. In this case the depth-dose distribution is scaled by the projected water-equivalent range of each dose grid spot. This approach is clearly valid only for a parallel beam with a small angular divergence like the one at PSI.

Equation (1) becomes

$$D(x, y, z) = N_{\mathrm{p}^+}\mathrm{ID}(\mathrm{wer})\frac{1}{2\pi\sigma_x\sigma_y}\exp[-(x_0 - x)^2/2\sigma_x^2]\exp[-(y_0 - y)^2/2\sigma_y^2] \qquad (2)$$

where

$$\mathrm{wer} = \mathrm{wer}(x, y, z)$$
$$\sigma_i = \sigma^W(\mathrm{wer}(x, y, z)) \quad \text{with} \quad i = x, y.$$

Thus the variation in the energy loss of the protons due to heterogeneous structures is modelled as a parallel projection of the density. However, all disturbance of the dose distribution behind

the interface due to the angular spread in the phase space and multiple Coulomb scattering are neglected in this approach.

3.2. A modified ray casting model including a correction for range dilution

Behind a density interface a change of the energy spectrum of the protons occurs which caused by the fact that they travel along different trajectories (Schneider and Pedroni 1995). This can be modelled as a dilution of the residual range of the protons. For a further improvement of the ray casting dose model, the effect of range dilution on the dose has been included in the algorithm through the use of the different depth-dose look-up tables (figure 3) described in section 2.2. The change in the beam width look-up-table due to range dilution is neglected. Conceptually this model is similar to the one described recently by Schneider *et al* (1998).

Thus, the integral dose ID(wer) which in formula (1) depends only on the water-equivalent range is now substituted by the integral dose tabulated as a function of the mean water-equivalent range and the range dilution for each individual dose calculation point:

$$D(x, y, z) = N_{\mathrm{p^+}}\mathrm{ID}(\overline{\mathrm{wer}}, \sigma_{\mathrm{RD}})\frac{1}{2\pi\sigma_x\sigma_y}\exp[-(x_0 - x)^2/2\sigma_x^2]\exp[-(y_0 - y)^2/2\sigma_y^2] \qquad (3)$$

where

$$\overline{\mathrm{wer}} = \overline{\mathrm{wer}}(x, y, z)$$
$$\sigma_i = \sigma_i^W(\overline{\mathrm{wer}}(x, y, z)) \quad \text{with} \quad i = x, y.$$

3.3. A pencil beam model based on the total proton fluence (fluence-dose model)

Another way of coping with the error introduced into the original scanned beam dose model by a large phase space is to split the scanned pencil beam into elemental pencil beams. New codes being written for broad beam proton dose calculations nowadays use similar methods (Petti 1992, 1996, Hong *et al* 1996). They are conceptually the same as pencil beam models used in photon dose calculation algorithms (Mohan *et al* 1986, Mackie *et al* 1985, Ahnesjö *et al* 1992). Their basic feature is the convolution of the proton fluence Φ with an elemental pencil beam dose distribution or dose kernel K, which describes the dose as deposited in water by an infinitesimally narrow proton pencil beam. The dose kernels are calculated using the original model of section 2.1 with the only exception that the contributions to the phase space of the beam entering into the patient are set to zero. As before, density heterogeneities are taken into account only along the central axis of the elemental pencil beam.

At PSI we implemented an elemental pencil beam dose model specific for the spot-scanning method. Theoretically it is possible to split the scanned beam up into a number of elemental pencil beams. This would multiply the computing time by that number. Since one field may contain many thousands of beam spots and an optimization typically consists of 100 loops each with a full dose calculation this requires a lot of computing power.

If an iterative spot by spot calculation is not needed, the computing time can be reduced by summing up the contributions of all beam spots to the total proton fluence at a point (neglecting its angular spread) prior to the convolution with the dose kernel. The characteristics of the kernel depend on the energy of the beam entering into the patient, which is a function of the number of range shifter plates (N_{RS}) used (dose kernel $K = K(x, y, \mathrm{wer}; N_{\mathrm{RS}})$). Therefore only fluence contributions from beam spots applied with the same number of range shifter plates can be convolved together (proton fluence $\Phi = \Phi(x, y, z; N_{\mathrm{RS}})$). The total dose is calculated at the end by a summation of all dose components.

For simplicity the equation below is given only for the calculation of the dose deposited by the subset of pencil beams applied with the same number of range shifter plates. Since the calculation is done on a discrete grid, the integrals in the convolution become sums

$$D(x, y, z; N_{\mathrm{RS}}) = \sum_{\tilde{y}} \sum_{\tilde{x}} \Phi(x - \tilde{x}, y - \tilde{y}, z; N_{\mathrm{RS}}) K(\tilde{x}, \tilde{y}, \mathrm{wer}(\tilde{x}, \tilde{y}, z); N_{\mathrm{RS}}). \quad (4)$$

In the calculation of the kernel, the total dose in each slice is normalized to become the integral dose from the look-up table.

As the spread of the beam due to the effective phase space is included in the calculation of Φ, the beam width (σ_{MCS}) for the calculation of the kernel is given only by the width due to multiple Coulomb scattering (MCS) in the patient. This is the only model presented here where fluence and dose calculation are performed separately. It is therefore called the fluence-dose calculation.

4. Results

4.1. Results of the models in a geometric phantom

The results obtained by the three models for the situation presented in figure 1 are shown now in figure 4. As expected, the ray casting model leads to a very sharp edge in the shadow of the slab due to the absence of angular spread effects (see isodose plot of figure 4A). Yet this algorithm is an improvement compared with the original scanned beam model. In the result of the modified ray casting model, the sharp edge is smoothed due to the range dilution correction (figure 4B). The result of the fluence-dose calculation (figure 4C) was obtained by simulating individual elemental pencil beams at each millimetre. The isodose plot for this situation is in good agreement with the result of the Monte Carlo simulation (figure 1B). Yet the shadowing effect from the slab in the peak region was found to be underestimated (see also section 5).

Further dose calculations were performed with the high-density slab simulated at different depths in the same homogeneous water phantom. Contrary to the situation shown in figure 2 and figure 4, the single beam of 177 MeV protons was simulated without range shifter plates and an air gap.

We chose to calculate the total squared differences (Δ_{sq}) between analytical and Monte Carlo simulated results as a measure for the overall accuracy. In figure 5 Δ_{sq} is plotted as a function of the position of the slab in depth for the three models.

The results for the two extreme positions of the high-density slab (below the surface of the phantom and directly in front of the Bragg peak) were further analysed by calculating the difference between the result of the Monte Carlo simulation and the analytical models for all voxels. Those differences are displayed normalized to the peak dose as histograms in figure 6 and the differences in a plane through the axis of the beam as grey-scale images in figure 7.

4.2. Results in anatomic situations

Different anatomical cases were studied to compare the three algorithms with each other. These cases are

(i) A concave meningioma wrapped around a critical structure in the lower part of the brain treated with a beam angled at 60° from frontal. The beam is parallel to a long bony structure which is expected to cause problems in the dose calculation.

(ii) A chordoma in the base of the skull region, treated with a frontal beam through the nasal cavities, which is not an optimal treatment angle but serves our purpose of selecting geometrically different distributions of heterogeneous structures.

(iii) A carcinoma of the prostate treated with a lateral beam through the femoral heads.

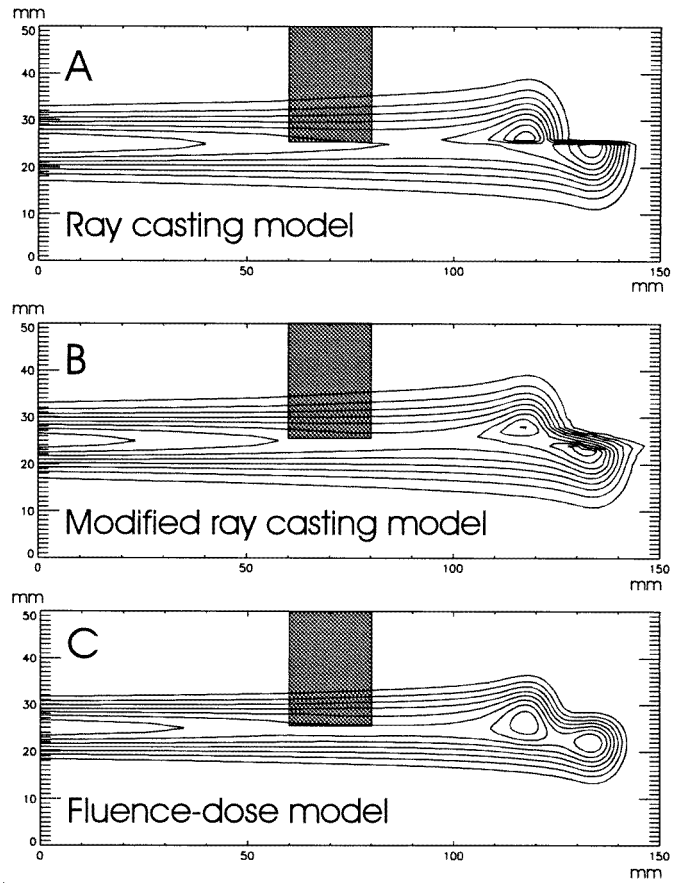

Figure 4. A first step to improving the scanned beam model (figure 1A) is achieved through a scaling of the dose distribution in depth along parallel rays as a function of the integral density. The result of this ray casting model is shown in A. Another step is achieved with the modified ray casting model (B), which smoothes the sharp, non-physical edge behind the interface. Finally, the situation is modelled best by the fluence-dose calculation (C) which is based on the summation of elemental parallel pencil beams. All parameters are the same as for figure 1.

Contour plots of the dose distributions show only minor differences between the algorithms and are therefore not displayed. As a measure for the overall accuracy error histograms like those in figure 6 are shown in figure 8 for the three cases.

5. Discussion

5.1. Accuracy of the models

From the results shown in figure 4 one tends to conclude that the fluence-dose model leads to the most accurate results. Although its results are generally rather accurate, the analysis of results for different geometrical situations shows that this is not true for all cases. A more detailed analysis is therefore needed.

The graph in figure 5 gives a good overview of the overall accuracy of the three models in the presence of a high-density slab at different positions in depth. The accuracy of the fluence-

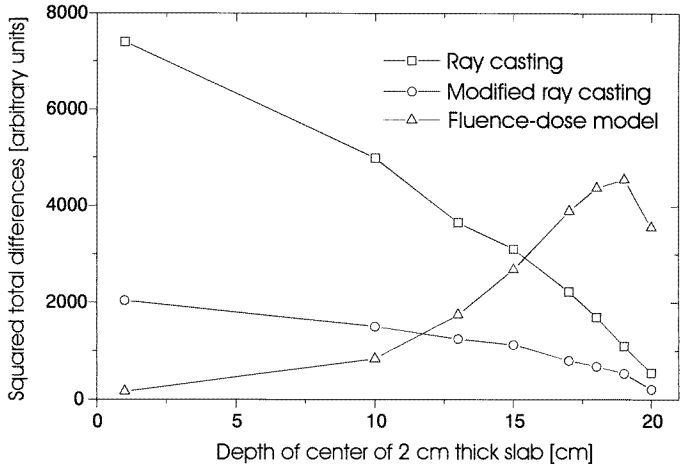

Figure 5. Total squared differences between analytical models and Monte Carlo simulation as a function of the position of a high-density slab. The initial energy is 177 MeV, which corresponds to a range of the protons in water of 21 cm. Clearly, the accuracy of the ray casting models increases the closer the slab position is to the Bragg peak. The difference between the two ray casting models is due to range dilution correction. The fluence-dose model on the other hand gives the best results when the slab is positioned far from the Bragg peak.

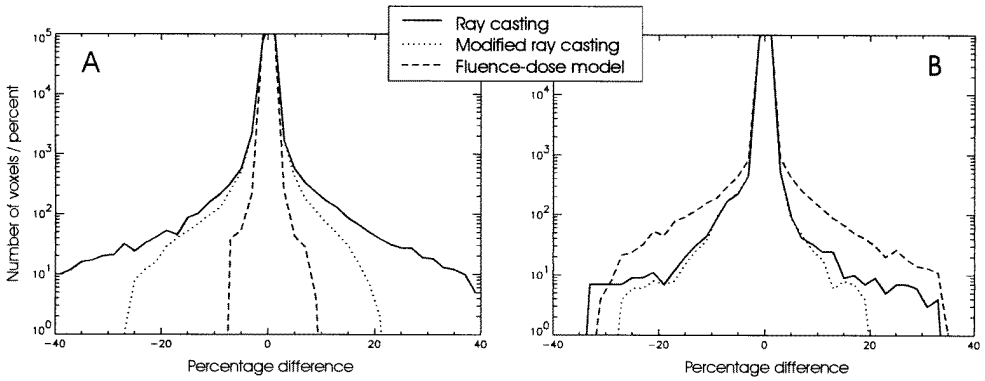

Figure 6. Statistical analysis of differences between analytical calculation and Monte Carlo simulation for two extreme positions of the slab. Clearly, the fluence-dose model is more accurate in situation A (slab below the surface), while the ray casting models are superior in case B (slab directly in front of the peak). Note the logarithmic scale.

dose model is very good compared with the Monte Carlo simulated results, if the distance between the inhomogeneity and the Bragg peak is large. However, it becomes increasingly worse the closer the inhomogeneity lies to the peak. The accuracy of both ray casting models, on the other hand, increases as the distance from the inhomogeneity decreases. When the high-density slab is sufficiently close to the position of the Bragg peak, the overall accuracy of both ray casting models is better than the accuracy of the fluence-dose model. This graph (figure 5) also shows the improvement from the ray casting model to the modified ray casting model using the range dilution correction. The same conclusions can be drawn from figure 6, while figure 7 gives more information about the location of the highest dose errors.

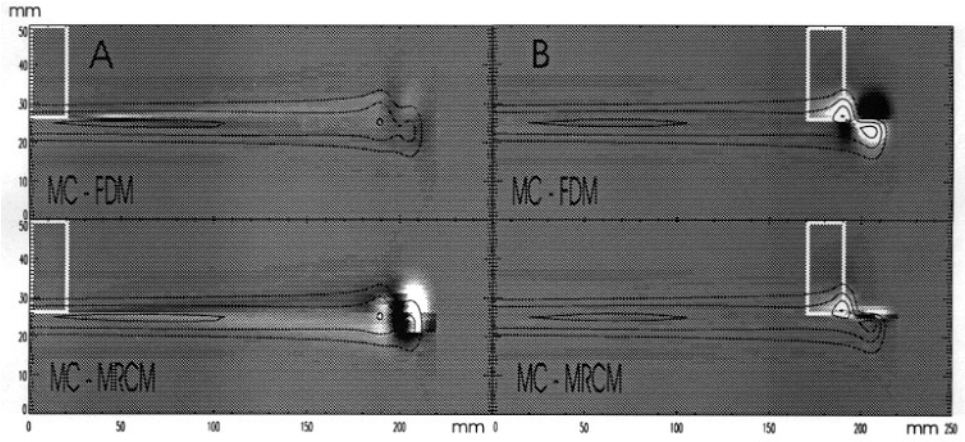

Figure 7. Differences between Monte Carlo (MC) results and analytical dose calculation for the fluence-dose model (FDM) and modified ray casting model (MRCM). In the black areas the Monte Carlo result is >10% lower than the analytical calculations, in the white areas it is >10% higher. The two images left (A) show the situation with the high-density slab below the surface, in the images on the right side (B) the slab is positioned directly in front of the peak. The isodose contours are taken from the Monte Carlo dose distribution. Note that the scaling is not the same in x and z.

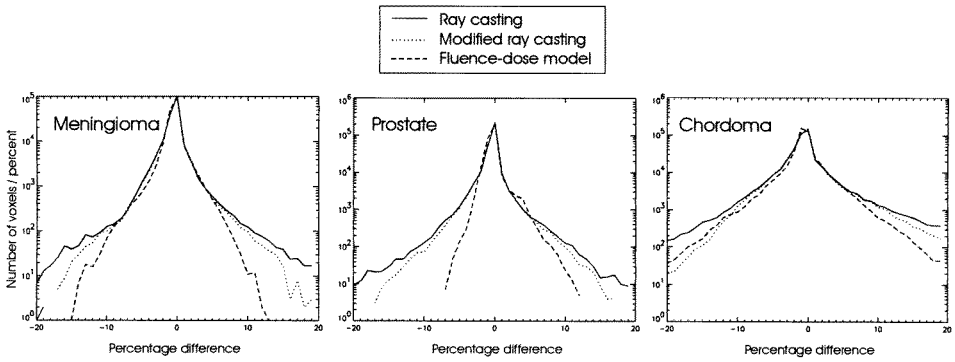

Figure 8. Histogram of differences between Monte Carlo simulation and the three analytical models for a meningioma, a chordoma and a prostate case. In most clinical cases the fluence-dose calculation was found to give the best results.

When the slab is directly below the surface (position 1 cm in figure 5, figure 6 and figure 7 case A), the fluence-dose model (FDM) leads to an almost perfect result. In the Bragg peak the differences between the results of the Monte Carlo simulation and the fluence-dose model do not exceed 3% of the peak dose. Errors larger than 5% occur only directly behind or along the interface. When the slab is very close to the position of the peak (position 18 cm, case B), the scattering behind the interface is overestimated by the fluence-dose model because the heterogeneities are only taken into account along the central axis of the elemental pencil beam.

The modified ray casting (figure 7, MRCM) models the shadowing of the inhomogeneity close to the Bragg peak better, but underestimates the effects of increased scattering towards the end of the proton range.

It is evident that the position in depth of the high-density inhomogeneity has a strong influence on the dose distribution in the region of the Bragg peak. Figure 9A shows a

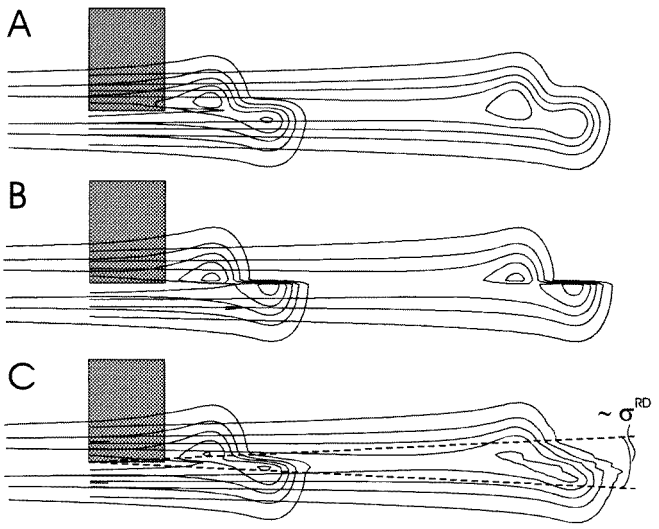

Figure 9. The effect of the position of the slab in depth on the results of the two ray casting dose calculations. The isodose curves are plotted relative to the slab position while the initial energy of the beam was kept constant. A: The results of the Monte Carlo calculation for the two situations. B: Ray casting model: the result is independent of the position of the slab. C: Range dilution corrected ray casting: the result depends on the position. The result of the fluence-dose calculation is not shown here. Its results are, however, independent of the slab position.

comparison between Monte Carlo calculated dose distributions for different positions of the slab in an otherwise homogeneous phantom. The isodose contours are plotted relative to the slab position. The sharpness of the shadow changes with the distance of the peak from the slab. Of the analytical models, only the modified ray casting model can simulate this dependency. Due to the sampling of angularly displaced rays, the area affected by the range dilution and integral density corrections increases with the distance from the slab. Consequently the dose distributions obtained from the modified ray casting differ depending on the position of the slab (figure 9C). In the area between the two broken curves the effect of the range dilution correction is clearly seen.

The conclusions drawn from the geometrical cases are also true in anatomical situations. Overall, the fluence-dose calculation models most of these situations best. In the meningioma case the number of voxels with errors above 5–10% is reduced remarkably by the fluence-dose model. In the difference histograms of a prostate case with a beam planned to come laterally through the hip, a considerable improvement can be achieved using the fluence-dose calculation, since the position of the inhomogeneity lies at some distance from the target. In a chordoma case, however, where a beam was planned through the nasal cavities, the overall performance of all analytical algorithms is more or less the same. The modified ray casting model always yields better results than the unmodified ray casting model. The differences are, however, smaller than expected from the results in the geometrical cases.

The remarks made above for the slab geometry concerning the performance of the analytical algorithms depending on the position of heterogeneous structures is also valid for anatomical cases (Schaffner 1997). Depending on the position of the target relative to the heterogeneities, errors in the calculated dose can appear inside or outside the target. In the above cases the percentage of the target volume with the dose over- or underestimated by 5%

and more are for the modified ray casting model 7.1%, 12.2% and 34.5% for meningioma, prostate and chordoma respectively and for the fluence-dose model 9.6%, 1.0% and 39.8%. These figures indicate that the fluence-dose model is not necessarily always the best choice.

5.2. Interpretation of the results

The real difference between the different models is given by the different way of treating the 'shadowing-effects' of inhomogeneities on the dose distribution (dose shadow) and how they propagate in combination with multiple Coulomb scattering in the patient (the 'sharpness' of the dose shadow). It is practically impossible to treat this problem exactly.

In both the unmodified ray casting and fluence-dose model the dose at a point is calculated using only the integral of the density up to that point. The information on the position of the inhomogeneity in depth is therefore not used.

Both models represent two extreme situations. The unmodified ray casting model produces a sharp shadow but neglects its deterioration with increasing depth through MCS in the patient. From the practical point of view it is as if we were to concentrate the totality of the density inhomogeneities (the differences to water) in the pixel in front of the point where the dose calculation is done.

The fluence model considers the full deterioration of the dose shadows from the patient's surface. From the practical point of view, it is as if the inhomogeneities were to be completely located at the surface of the patient.

The only way to improve these models is to consider modifications of the models which take into account the location of the inhomogeneities in depth. The range dilution correction applied to the ray casting model is the most reasonable first step in this direction.

The result is better with the unmodified ray casting model, but that model is not perfect either. The weakness here is given by the fact that only straight trajectories are used as representative rays. It is not clear to us how we could further improve the fluence-dose model in the same direction without prohibitively increasing the calculation time. We are therefore left with two alternative calculation models, which are complementary to each other and which describe the dose distribution best at following extreme situations:

(i) The modified ray casting model when the inhomogeneities are close to the Bragg peak.
(ii) The fluence model when the inhomogeneity is close to the surface of the patient.

5.3. Practical use of the models

Our dose calculation algorithms are used in two different phases of the treatment planning process. For the optimization loop the scanned beam must be modelled completely at each iteration. The models we use for this phase are the two ray casting models, since it is desirable to use a fast algorithm for the optimization. The cost in terms of computing time for the range dilution correction is relatively low. The calculation of the mean range and the range dilution correction takes considerably more time than the nominal range calculation, which is used in the unmodified ray casting model. It is, however, done only once and in advance of the optimization procedure which is the most time-consuming process of the planning. The time needed for an optimization loop is exactly the same for both ray casting models.

For the final dose calculation any model—including the fluence-dose calculation and the Monte Carlo simulation—can be used. While the Monte Carlo simulation is expected to produce the most accurate results, the fluence-dose model is considerably faster and is a very good model for situations with inhomogeneities close to the surface. Generally, it is expected that the fluence-dose and ray casting models exaggerate errors in opposite directions. They

are therefore complementary to each other. If a Monte Carlo simulation is not performed, it is very useful to use both models and compare their results.

The simulation of collimators presents a situation similar to the one with the slab at the surface of the phantom. The modelling of collimators is therefore best done by using the fluence-dose model. Collimators are needed in scattered beam techniques to conform the dose laterally to the target. At PSI there are plans to install optionally collimators (Pedroni *et al* 1995) in addition to the conformation by dynamic scanning to improve the lateral dose fall-off in the treatment of superficial tumours. The need to simulate the effects of a collimator was another reason to develop the fluence-dose model.

6. Conclusions

It has been shown that a ray casting dose calculation specialized for spot-scanning can already predict the influence of density inhomogeneities on the dose distribution reasonably well. Further improvements have been achieved by using a range dilution correction to the ray casting model. Both these models are implemented in the optimization routine for the beam spots which allows us to make full use of the intrinsic intensity modulation capabilities of the spot-scanning technique. In situations with inhomogeneities close to the surface, an elemental pencil beam model yields the best results. This model is also expected to best model the influence of collimators. No single model is capable of predicting the correct dose in any situation. The models are complementary to each other. It is therefore important to have all of them available. Above a certain level of complexity it is, however, preferable to use a Monte Carlo calculation for the final evaluation of the dose distribution.

References

Ahnesjö A, Saxner M and Trepp A 1992 A pencil beam model for photon dose calculation *Med. Phys.* **19** 263–73

Bichsel H 1972 Passage of charged particles through matter *American Institute of Physics Handbook* (New York: McGraw-Hill) pp 8-142–8-185

Chen G T Y, Rajinder P S, Castro J R, Lyman J T and Quivey J M 1979 Treatment planning for heavy ion radiotherapy *Int. J. Radiat. Oncol. Biol. Phys.* **5** 1809–19

Hong L, Goitein M, Bucciolini M, Comiskey R, Gottschalk B, Rosenthal S, Serago C and Urie M 1996 A pencil beam algorithm for proton dose calculations *Phys. Med. Biol.* **41** 1305–30

Koehler A M, Schneider R J and Sisterson J M 1975 Range modulators for protons and heavy ions *Nucl. Instrum. Methods* **131** 437–40

Lomax A 1999 Intensity modulation methods for proton radiotherapy *Phys. Med. Biol.* **44** 185–205

Lomax A, Pedroni E, Schaffner B, Scheib S, Schneider U and Tourovsky A 1996 3D treatment planning for conformal proton therapy by spot scanning *Proc. 19th L H Gray Conf.* (London: British Institute of Radiology) pp 67–71

Mackie T R, Scrimger J W and Battista J J 1985 A convolution method of calculating dose for 15-MV x-rays *Med. Phys.* **12** 188–96

Mohan R, Chui C and Lidovsky L 1986 Differential pencil beam dose computation model for photons *Med. Phys.* **13** 64–73

Øverås H 1960 Small angle multiple scattering in confined bodies *CERN Yellow Report* 60-18

Pedroni E *et al* 1995 The 200 MeV proton therapy project at the Paul Scherrer institute: conceptual design and practical realization *Med. Phys.* **22** 37–53

Petti P 1992 Differential-pencil-beam dose calculations for charged particles *Med. Phys.* **19** 137–49

——1996 Evaluation of a pencil-beam dose calculation technique for charged particle radiotherapy *Int. J. Radiat. Oncol. Biol. Phys.* **35** 1049–57

Ragona R, Rolando V and Solano A 1997 Treatment planning of proton beams using the GEANT Monte Carlo *Advances in Hadrontherapy* ed U Amaldi *et al* (Amsterdam: Excerpta Medica Elsevier) pp 304–8

Schaffner B 1997 Range precision of therapeutic proton beams *PhD Thesis* ETH Zürich

Scheib S 1993 Spot-Scanning mit Protonen: Experimentelle Resultate und Therapieplanung *PhD Thesis* ETH Zürich

Scheib S and Pedroni E 1992 Dose calculations and optimisation for 3D conformal voxel scanning *Radiat. Environ. Biophys.* **31** 251–6

Scheib S, Pedroni E, Lomax A, Blattmann H, Böhringer T, Coray A, Lin S, Munkel G, Schneider U and Tourovsky A 1994 Spot scanning with protons at PSI: experimental results and treatment planning *Hadrontherapy in Oncology* ed U Amaldi and B Larsson (Amsterdam: Excerpta Medica Elsevier) pp 471–80

Schneider U and Pedroni E 1995 Proton radiography as a tool for quality control in proton therapy *Med. Phys.* **22** 353–63

Schneider U, Schaffner B, Lomax A, Pedroni E and Tourovsky A 1998 A technique for calculating range spectra of charged particle beams distal to thick inhomogeneities *Med. Phys.* **25** 457–63

Tourovsky A, Pedroni E and Schneider U 1993 Monte Carlo codes for proton radiography and treatment planning *PSI Life Sci. Newsletter* 20–2

Urie M, Goitein M, Holley W R and Chen G T Y 1986 Degradation of the Bragg peak due to inhomogeneities *Phys. Med. Biol.* **31** 1–15

Urie M, Goitein M and Wagner M 1984 Compensating for heterogeneities in proton radiation therapy *Phys. Med. Biol.* **29** 553–66